

This is the accepted manuscript made available via CHORUS. The article has been published as:

Intersubband resistance oscillations in crossed electric and magnetic fields

Scott Dietrich, Sean Byrnes, Sergey Vitkalov, A. V. Goran, and A. A. Bykov

Phys. Rev. B **86**, 075471 — Published 31 August 2012

DOI: [10.1103/PhysRevB.86.075471](https://doi.org/10.1103/PhysRevB.86.075471)

Inter-subband resistance oscillations in crossed electric and magnetic fields

Scott Dietrich, Sean Byrnes, and Sergey Vitkalov*

Physics Department, City College of the City University of New York, New York 10031, USA

A. V. Goran and A. A. Bykov[†]

Institute of Semiconductor Physics, 630090 Novosibirsk, Russia

(Dated: July 23, 2012)

Quantum oscillations of nonlinear resistance are investigated in response to electric current and magnetic field applied perpendicular to single GaAs quantum wells with two populated subbands. At small magnetic fields current-induced oscillations appear as Landau-Zener transitions between Landau levels inside the lowest subband. The period of these oscillations is proportional to the magnetic field. At high magnetic fields, a different kind of quantum oscillations emerges with a period, that is independent of the magnetic field. At a fixed current the oscillations are periodic in inverse magnetic field with a period that is independent of the *dc* bias. The proposed model considers these oscillations as a result of spatial variations of the energy separation between two subbands induced by the electric current.

PACS numbers: 72.20.Mj, 73.43.Qt, 73.50.Jt, 73.63.Hs

I. INTRODUCTION

The magnetotransport phenomena in high-mobility, modulation-doped semiconductor structures are commonly studied with only one populated subband (E_1), because the electron mobility decreases with filling the second subband (E_2) due to inter-subband scattering¹. The latter also gives rise to magneto-inter-subband oscillations (MISO) of the dissipative resistance². In electron systems with two populated subbands MISO have maxima in magnetic fields B satisfying the relation³⁻⁵: $\Delta_{12} = l \cdot \hbar\omega_c$, where $\Delta_{12} = E_2 - E_1$ is the energy separation of the bottoms of the subbands, $\omega_c = eB/m^*$ is cyclotron frequency, m^* is effective electron mass and l is a positive integer. In contrast to Shubnikov de Haas (SdH) oscillations the MIS-oscillations exist at high temperature $kT > \hbar\omega_c$. An interference of these oscillations with phonon-induced oscillations has been reported⁶.

At small quantizing magnetic fields a finite electric current induces several additional nonlinear phenomena. At low temperatures small currents considerably decrease the resistance. The dominant mechanism inducing the resistance drop is a peculiar Joule heating (quantal heating), which produces a non-uniform spectral diffusion of electrons over the quantized spectrum. The spectral diffusion is stabilized by inelastic processes ("inelastic" mechanism)⁷. The heating has been recently observed and studied⁸⁻¹¹. At higher currents electron transitions between Landau levels occur due to an elastic electron scattering on impurities in the presence of an electric field^{12,13}. The transitions increase the resistance, which was observed in electron systems both with a single occupied subband¹⁴⁻¹⁶ and with multi-subband occupation¹⁷⁻²⁰. In the latter case, an interference of the magneto-inter-subband quantum oscillations (MISO) with the current induced inter-level scattering was reported.

Recent investigations of the nonlinear transport in

stronger magnetic fields reveal another kind of current-induced resistance oscillations in electron systems with a single band occupation²¹. These oscillations occur in electric fields that are significantly smaller than the one required for the current-induced Landau-Zener transitions between Landau levels¹². The period of these current-induced oscillations is found to be independent of the magnetic field. The oscillations are considered to be a result of spatial variations of the electron filling factor (electron density δn) with the applied electric field.

In this paper we report an observation of current-induced resistance oscillations of the dissipative resistance in electron systems with two populated subbands. Two kinds of oscillations are detected. At small magnetic fields we observed resistance oscillations with a period proportional to the magnetic field. We found that these oscillations are related to the current-induced Landau-Zener transitions between Landau levels^{12,17,19}. At higher magnetic fields another type of the resistance oscillations emerges with a period that is independent of the magnetic field. In the paper these oscillations are studied at high temperatures at which only MIS-oscillations are present.

Despite a similarity between the current-induced oscillations with the B-independent period, which are found in single subband systems²¹ and the oscillations reported in this paper, there is at least one distinct feature to distinguish the two. Namely the oscillations in the two-subband systems occur at high temperatures $kT \gg \hbar\omega_c$ and, therefore, the total number of the electron states carrying the electric current (inside the energy interval kT) does not oscillate with the Fermi energy (in other words with the total electron density n). In this regime the SdH oscillations are damped and in single subband systems the current-induced oscillations are absent²¹. Thus even if both kinds of observed oscillations have a common origin, the oscillations reported in this paper are not directly (simply) related to the spatial vari-

ations of the electron density δn induced by the electric current. Another interesting feature is the phase of these oscillations. The oscillations appear to be quasi-periodic with respect to the applied current but with an apparent π -phase shift with respect to the zero bias. Below we present our findings and provide an interpretation of the obtained results.

II. EXPERIMENTAL SETUP

Our samples are high-mobility GaAs quantum wells grown by molecular beam epitaxy on semi-insulating (001) GaAs substrates. The width of the GaAs quantum well is 13 nm. Two AlAs/GaAs type-II superlattices grown on both sides of the well served as barriers, providing a high mobility of 2D electrons inside the well at a high electron density²². Two samples were studied with electron density $n_{1,2} = 8.09 \times 10^{15} \text{ m}^{-2}$ and mobility $\mu_1 = 121 \text{ m}^2/\text{Vs}$ and $\mu_2 = 73 \text{ m}^2/\text{Vs}$.

The studied 2D electron systems are etched in the shape of a Hall bar. The width and the length of the measured part of the samples are $d = 50 \mu\text{m}$ and $L = 450 \mu\text{m}$. To measure the resistance we use the four point probe method. Direct electric current I_{dc} (dc bias) is applied simultaneously with 12 Hz ac excitation I_{ac} through the same current contacts (x -direction). The longitudinal ac (dc) voltage V_{xx}^{ac} (V_{xx}^{dc}) is measured between potential contacts displaced $450 \mu\text{m}$ along each side of the sample. The Hall voltage V_H is measured between potential contacts displaced $50 \mu\text{m}$ across the electric current in y -direction.

The current contacts are separated from the measured area by a distance of $500 \mu\text{m}$, which is much greater than the inelastic relaxation length of the 2D electrons $L_{in} = (D\tau_{in})^{1/2} \sim 1 - 5 \mu\text{m}$. The longitudinal and Hall voltages were measured simultaneously, using two lockin amplifiers with $10 \text{ M}\Omega$ input impedances. The potential contacts provided insignificant contribution to the overall response due to small values of the contact resistance (about $1 \text{ k}\Omega$) and negligibly small electric current flowing through the contacts.

Measurements were taken at different temperatures and magnetic fields in a He-3 insert inside a superconducting solenoid. Samples and a calibrated thermometer were mounted on a cold copper finger in vacuum. The magnetic field was applied perpendicular to the 2D electron layers.

III. RESULTS

Figure 1 presents the dependence of the dissipative resistance on the magnetic field at temperature $T = 4.35 \text{ K}$. At this temperature $kT > \hbar\omega_c$ and Shubnikov de Haas oscillations are suppressed at $B < 0.5 \text{ T}$. The maximums of the observed magneto-intersubband oscillations (MISO) are due to the enhancement of elastic electron scattering,

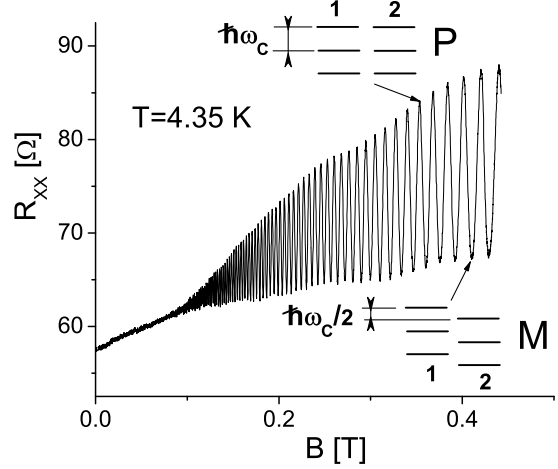


FIG. 1: Dependence of the resistance R_{xx} on magnetic field with no dc bias applied. Sample N1.

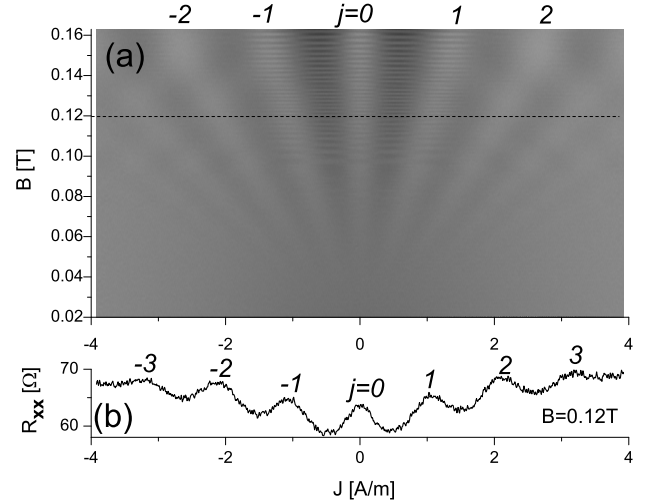


FIG. 2: a) Dependence of differential resistance R_{xx} on magnetic field and averaged density of electric current J ; (b) Dependence of the resistance on the current density J at fixed magnetic field as labeled. Index $j = \pm 1, \pm 2, \dots$ numerates Landau-Zener transitions inside lowest subband, which obey Eq.(1). $T = 5.1 \text{ K}$. Sample N1.

which occurs when the Landau levels in two subbands are lined up with each other (state P in Fig.1). At this condition elastic electron transitions occur between the subbands, increasing the total electron scattering rate and, thus, the resistance. Minima of the oscillations occur when the Landau levels in one subband are between the levels of another subband. In this condition the elastic electron scattering between subbands is suppressed (state M in Fig.1)⁵.

Figure 2(a) presents differential resistance R_{xx} at different averaged density of the electric current $J =$

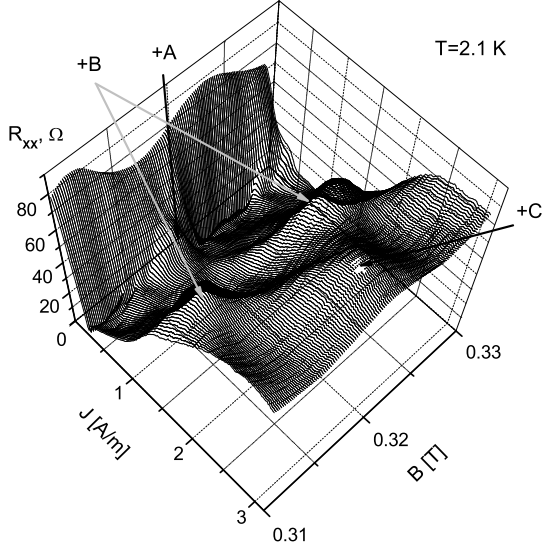


FIG. 3: Dependence of resistance R_{xx} on magnetic field and current density J . Labels +A, +B and +C indicate different maxima induced by dc bias. $T=2.1$ K. Sample N1.

$I_{dc}/(d = 50\mu)$ and small magnetic fields. The differential resistance oscillates with the dc bias. An example of the oscillations is shown in figure 2(b) at fixed magnetic field $B=0.12$ Tesla. The dependence is a horizontal cut of the 2D plot and is shown by the dashed line in Fig.2(a). The position of a resistance maximum j is proportional to the magnetic field and satisfies the following relation:

$$2eE_j R_c^{(1)} = j \cdot \hbar\omega_c, \quad (1)$$

where E_j is the electric field (mostly the Hall electric field in the sample) corresponding to the maximum j , $R_c^{(1)}$ is the cyclotron radius of electrons in the first subband (the lowest subband) and $j = 0, 1, 2, \dots$ is an integer. Eq.(1) describes Landau-Zener transitions between Landau levels in the first subband¹².

At a higher resolution the data shows oscillations of the magnitude of the maxima $j = \pm 1$ with the magnetic field at $B > 0.1$ (T). The oscillations are periodic in inverse magnetic field and are in-phase with the intersubband oscillations at zero dc bias ($j = 0$). Similar oscillations are observed for the minimum between $j = 0$ and $j = \pm 1$ maxima. These oscillations are shifted by phase π with respect to the oscillations of the maxima $j = 0, \pm 1$. The observed oscillations appear as an interplay between the dc bias induced Landau-Zener transitions between Landau levels inside the lowest subband and the intersubband transitions, which are periodic in inverse magnetic field $1/B$. At higher dc biases ($|j| > 1$) the amplitude modulation with the $1/B$ periodicity disappears. In particular no amplitude modulation is found for $j = \pm 2, 3$ maxima.

Figure 3 presents a typical nonlinear response at a high

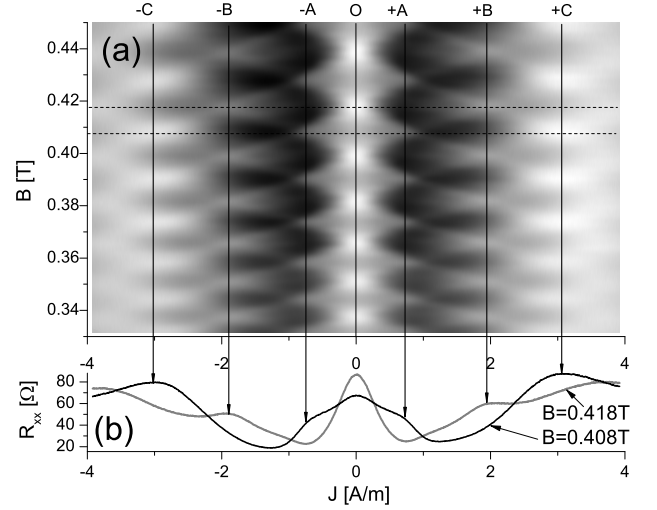


FIG. 4: (a) Dependence of resistance R_{xx} on magnetic field and current density J , indicating strong correlation of features $\pm A$ and $\pm C$ with MISO minima and features $\pm B$ with MISO maxima. (b) Dependence of R_{xx} on current density J at magnetic field $B=0.418$ T corresponding to MISO maximum and at magnetic field $B=0.408$ T corresponding to MISO minimum. $T=4.7$ K. Sample N1.

magnetic field. The response is symmetric with respect to applied dc bias and is shown for the positive bias. There are several distinct features, which appear with the dc bias. The features are labeled in the figure. Firstly, we discuss the evolution of the resistance with the dc bias at the minimum of a MIS oscillation (state M in fig.1). When the dc bias is applied, the resistance falls down and, then, develops a shoulder labeled by symbol +A. The initial drop of the resistance is mostly due to the quantal heating. Further increase of the dc current leads to formation of a maximum labeled by symbol +C.

When the dc bias is applied to state P (see fig.1), corresponding to the maximum of a MIS oscillation, the resistance drops much more abruptly and significantly in comparison with the previous case. At low temperatures the resistance drop reaches zero and forms zero resistance state (ZDRS)^{18,23–25}. Further increase of the dc bias leads to the formation of a maximum labeled by symbol +B.

An evolution of the discussed features with the magnetic field is shown in figure 4(a). The figure demonstrates that the positions of all features ($\pm A$, $\pm B$, $\pm C$) are essentially independent of the magnetic field. Figure 4(b) presents horizontal cuts of the 2D plot through a maximum ($B=0.418$ T) and a minimum ($B=0.408$ T) of the inter-subband quantum oscillations.

Figure 5 presents an overall behavior of the quantum oscillations in a broad range of magnetic fields and dc biases. The data was obtained from sample N2. The figure shows the crossover of the intraband Landau-Zener transitions, obeying Eq.(1), and the oscillations marked as $\pm A$, $\pm B$, $\pm C$, which have the MISO periodicity. The

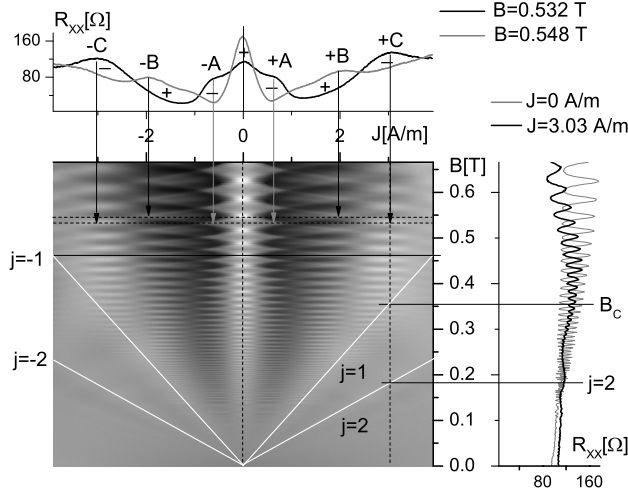


FIG. 5: Evolution of differential resistance with magnetic field and current density in broad range of magnetic fields. White straight lines indicate Landau-Zener transitions which obey Eq.(1). Upper panel presents horizontal cut through MISO maximum at $B=0.548\text{T}$ (gray line) and cut through MISO minimum at $B=0.532\text{ T}$ (black line). Sign $+$ ($-$) indicates regions of current density J , inside which the current-induced oscillations have $0(180)$ degree phase shift with respect to MIS-oscillations at $J=0\text{A/m}$. Right panel presents two vertical cuts of the 2D plot taken at current densities as labeled. Magnetic field dependence at $J=3.03\text{ A/m}$ indicates strong reduction of the resistance oscillations at $B < B_c$ inside the region corresponding to Landau-Zener transitions. $T=5\text{K}$. Sample N2.

apparent crossover occurs near the Landau-Zener transition corresponding to $j = \pm 1$. Namely the oscillations with $1/B$ MISO periodicity occurs at magnetic fields B_c corresponding to

$$\hbar\omega_c \geq 2eE_1 R_c^{(1)}. \quad (2)$$

At smaller magnetic fields ($B < B_c$) the oscillations are significantly reduced. Two vertical cuts of the 2D plot taken at different currents are shown in the right panel of Fig. 5. The curve taken at $J=3.03\text{ A/m}$ shows the strong reduction of the oscillations at $B < B_c$ in a comparison with the MISO at $J=0\text{A}$. Thus the main intraband Landau-Zener transition ($j = \pm 1$) forms a boundary below which the current-induced oscillations with $1/B$ intersubband periodicity are strongly damped.

The upper panel of Fig. 5 shows two horizontal cuts of the 2D plot. The black solid line presents the dependence of the resistance R_{xx} on dc bias taken at $B=0.532\text{T}$ corresponding to a minimum of MISO. The gray line presents the dependence taken at $B = 0.548\text{ (T)}$ corresponding to a MISO maximum. The two curves intersect at 8 points. These intersections marks the regions at which the oscillations with MISO periodicity changes their phase by π . At the intersections the oscillations are

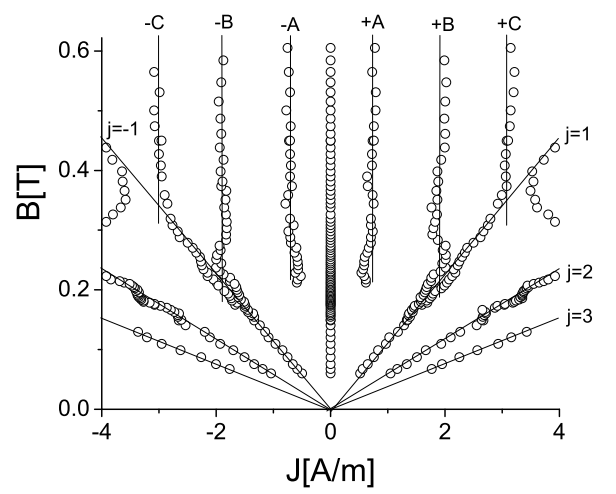


FIG. 6: Positions of resistance maximums and different magnetic fields and current density. Two kind of oscillations are observed: in magnetic fields at and below B_c , which satisfy Eq.(2), the maximums correspond to Landau-Zener transitions in lowest subband that obey Eq.(1). Solid straight lines at $j = \pm 1, 2$, and 3 represent the equation. At $B > B_c$ the resistance maximums follow the vertical solid lines representing features $\pm A, \pm B$ and $\pm C$ shown on Fig.3,4,5. The crossover between two kind of oscillations occurs at $B = B_c$ presented by line $j = \pm 1$. Sample N1.

nearly vanished. Sign $+$ indicates the region between two intersections in which the oscillations are in-phase with the MISO, whereas sign $-$ indicates the regions in which the oscillations are shifted by phase π with respect to the MISO.

Figure 6 presents an accurate position of the resistance maximums with $1/B$ periodicity at different currents and magnetic fields for sample N1. The figure indicates clearly that at $B = B_c$ ($j = \pm 1$) the resistance maximums follow the main Landau-Zener transition $j = \pm 1$ whereas at $B > B_c$ the maximums are nearly independent of magnetic field (features $\pm A, \pm B, \pm C$). The solid lines $j = \pm 1$ mark the boundary between the two kinds of oscillations. The lines obey eq.(1) at $j = \pm 1$ with the cyclotron radius R_c^1 corresponding to the lowest subband. The complete theory of the current-induced oscillations of the resistance of 2D electron system with two populated subbands is not available for a general case. The case of a bilayer electron system with two closely spaced and almost equally populated electronic subbands has been studied recently^{17,19}. These results are in qualitative agreement with the present data at small magnetic fields $B < B_c$.

At high magnetic fields $B > B_c$ figures 5 and 6 present a new kind of current-induced quantum oscillations. A striking feature of these oscillations is the independence of the position of these oscillations on magnetic field. An interesting property of these oscillations is the region in which the oscillations occur. Figures 5, 6 show that these

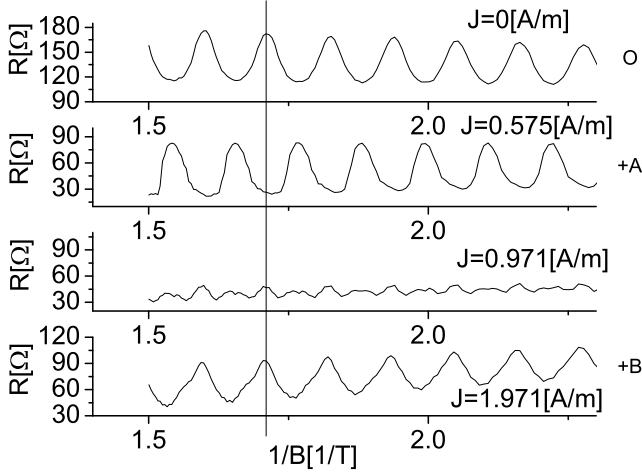


FIG. 7: Dependence of resistance on inverse magnetic field at different dc biases as labeled. $T=5$ K. Sample N2.

oscillations start at the line corresponding to Landau-Zener transitions at $j = \pm 1$ in the lowest subband and propagate to higher magnetic fields. Another interesting property is an apparent quasi-periodicity of the oscillations with applied current. Namely the features $\pm A$, $\pm B$, $\pm C$ are displaced by about the same value of the electric current density from each other: $\delta J \sim 1.27$ (A/m). The phase of the oscillations is shifted by π with respect to zero dc bias. It seems strange that the MIS-oscillations ($J=0$ (A/m)) are not a part of this periodic set.

Figure 7 demonstrates the $1/B$ periodicity and the phase of the current-induced oscillations at different dc biases as labeled. The figure indicates that oscillations at $J=1.97$ (A/m) (B+ feature) are in phase with MISO, whereas oscillations at $J=0.575$ A/m (A+ feature) are shifted by π with respect to MISO. Figure 7 shows also the strong reduction of the oscillations at $J=0.971$ A/m. At this current the oscillations change phase by π . The current corresponds to the intersection of two curves shown in upper panel of Fig.5.

The $1/B$ periodicity of the oscillations and the magnetic field independence of the electric current I_{dc} , inducing the oscillations at $B > B_c$, indicates a similarity of these quantum oscillations with the current-induced quantum oscillations reported recently in Ref.²¹. Below we consider a model, which is, in many respects, analogous to one described in Ref.²¹. The model reproduces the main properties of the observed quantum oscillations.

IV. MODEL AND DISCUSSION

Current-induced quantum oscillations with $1/B$ periodicity were recently observed in 2D electron systems with a single occupied subband²¹. The oscillations occur in a strong magnetic field at which Shubnikov de Haas

oscillations (SdH) are well developed²⁶. With respect to the electric current, the oscillations are periodic with a period that is independent of the magnetic field. The proposed model considers the oscillations as the result of a variation of the electron filling factor with the dc bias. In contrast to SdH oscillations, the variation appears across the sample and is related to a spatial change of the electron density δn . If the change δn is comparable with the number of electron states in a Landau level $n_0 = m/(\pi\hbar^2) \cdot \hbar\omega_c$, then one should expect a variation of the electron resistivity. The spatial variation of the resistivity leads to oscillations of the sample resistance²¹.

MIS-oscillations are due to a periodic enhancement of the inter-subband scattering, when Landau levels in two subbands are lined up as shown in Fig.1. MISO have maxima in magnetic fields B satisfying the relation³⁻⁵: $\Delta_{12} = l \cdot \hbar\omega_c$, where $\Delta_{12} = E_2 - E_1$ is the energy separation of the bottoms of the subbands and l is an integer. In contrast to SdH oscillations, the MIS-oscillations exist at high temperature $kT > \hbar\omega_c$ and are insensitive to variations of the Fermi energy and/or electron density n for non-interacting 2D carriers.

For interacting electron systems the situation is different. Recent direct experiment indicates that gap E_0 between conducting and valence bands of 2D electron systems formed in GaAs quantum wells depends considerably on the electron density n ²⁷. This observation opens a way to consider the dependence of the energy separation between two subbands Δ_{12} on the electron density as a mechanism leading to the current-induced quantum oscillations in magnetic fields $B > B_c$. Indeed the experiment Ref.²⁷ demonstrated about one percent change of the gap E_0 at a Hall voltage $V_H=75$ (mV) in magnetic field $B=0.3$ (T). The Hall voltage is comparable with the one observed in our experiment: $V_H \approx 50$ mV at $B=0.35$ (T) and $J=4$ (A/m). At $B=0.35$ (T) the phase of the MISO $2\pi\Delta_{12}/\hbar\omega_c \approx 2\pi \cdot 30$ requires about 3 percent change of the inter-subband energy separation Δ_{12} to make an additional MIS-oscillation cycle. The comparison indicates the feasibility of the proposed mechanism, taking into account that in our samples the GaAs quantum well is sandwiched between conducting layers, which enhance significantly the electron screening and, therefore, the variations of the electron density δn with the dc bias²¹.

In the model described below we assume that the dc bias-induced variation of the electron density $\delta n(r)$ changes the energy separation $\Delta_{12}(n)$ between two subbands across samples. Since relative variations of the electron density is small $\delta n/n \ll 1$, we will consider only the linear term of the dependence $\Delta_{12}(n)$:

$$\Delta_{12}(n) = \Delta_0 + \gamma\delta n(r), \quad (3)$$

where Δ_0 is the energy separation at zero dc bias and the parameter γ is a constant. The following consideration is qualitatively similar to the model described in detail in Ref.²¹. Below we describe the main parts of the model,

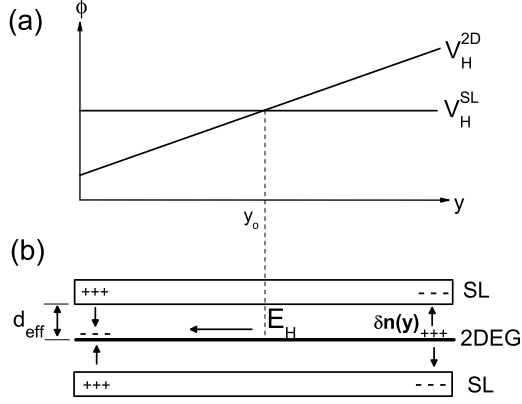


FIG. 8: Dependence of the electric potential on position y in the direction perpendicular to the electric current in strong magnetic field. Line V_H^{2D} describes the potential in GaAs quantum well, in which strong Hall effect is developed. Line V_H^{SL} describes the potential in the highly resistive superlattice layer, in which the Hall voltage is negligibly small due to the negligibly small current in the layer.

omitting some details.

The conducting 2D electron system in the GaAs quantum well is sandwiched between two layers of AlAs/GaAs superlattices (SL) of the second kind²². The parameters of the superlattices are adjusted to set the system close to a metal-insulator transition. At this condition, the barely-conducting SL layers efficiently screen electric charges but do not contribute considerably to the overall conductivity of the structure. Electric contacts connect the GaAs and the SL layers. Thus the system is considered as a set of parallel conductors. At zero magnetic field the distribution of the electric potential driving the current is the same in all layers due to the same shape of the conductors. That is to say at $B=0$ the potential difference between different layers is absent. In the poorly conducting SL layers the electric current is several order of magnitude smaller than the one in the highly conducting GaAs quantum well.

The layers have a different distribution of the electric potential in a strong magnetic field, at which $\omega_c \tau_{tr}^{2D} \gg 1$ and $\omega_c \tau_{tr}^{SL} \ll 1$, where τ_{tr}^{2D} and τ_{tr}^{SL} are transport times in the GaAs and in the SL layers. At $\omega \tau_{tr}^{2D} \gg 1$ the electric field in the GaAs layer is almost perpendicular to the current due to the strong Hall effect. In contrast the very small electric current in the SL layer induces a negligible Hall voltage. The Hall voltages are shown in Fig.8 (a) for small currents (linear response). Figure 8(b) presents distribution of electric charges in the structure. Electric charges are accumulated near the edges of the 2D highly conducting GaAs layer, inducing the Hall electric field E_H . The charges are partially screened by charges accumulated in the conducting SL layers.

Due to the small Hall voltage V_H^{SL} and the absence of the electric current across the system the change of the electric potential $\phi^{SL}(y)$ in the SL layer is negligibly small. Below we consider the potential ϕ^{SL} as a constant. Due to a finite screening length λ_s in the SL layer the charge accumulation occurs at a distance $d \sim \lambda_s$. Below we approximate the charge distribution by a charged capacitor with an effective distance d_{eff} between conducting plates.

The proposed model considers a long 2D Hall bar with a width L_y ^{28,29}. Electric current is in x -direction and the Hall electric field is in y -direction. In a long conductor the electric field $\vec{E} = (E_x, E_y)$ is independent of x , due to the uniformity of the system in the x direction:

$$\frac{\partial E_x}{\partial x} = \frac{\partial E_y}{\partial x} = 0 \quad (4)$$

For a steady current Maxwell equations yield:

$$\frac{\partial E_x}{\partial y} = \frac{\partial E_y}{\partial x} \quad (5)$$

Eq.(4) and eq.(5) indicate, that the x component of the electric field is the same at any location: $E_x = E = \text{const}$.

Boundary conditions and the continuity equation require that the density of the electric current in y direction is zero: $J_y = 0$ and therefore,

$$E_x = \rho_{xx} J_x \quad E_y = \rho_{yx} J_x \quad (6)$$

where ρ_{xx} and ρ_{yx} are longitudinal and Hall components of the resistivity tensor³⁰. We approximate the MIS-oscillations of the resistivity by a simple expression⁵:

$$\rho_{xx}(n(y)) = \rho_D [1 + A_{mis} \cdot \cos(\frac{2\pi \Delta_{12}}{\hbar \omega_c})] \quad (7)$$

where ρ_D is Drude resistivity, and A_{mis} describes the amplitude of the intersubband quantum oscillations. The amplitude is different from the amplitude of Shubnikov de Haas oscillations, since the two phenomena have a different origin⁵.

An electrostatic evaluation of the voltage between conducting layers, shown in Fig.8(b), yields:

$$\phi^{2D}(y) = \phi^{SL} + \frac{e \delta n(y) d_{eff}}{2 \epsilon \epsilon_0} \quad (8)$$

where ϕ^{2D} and ϕ^{SL} are electric potentials of the GaAs (2DEG) and superlattice (SL) layers, and ϵ is permittivity of the SL layer. Expressing the electron density δn in terms of electric potential ϕ^{2D} from Eq.(8) and substituting the relation into eq.(3) and then into eq.(7) one can find dependence of the resistivity on the electric potential: $\rho_{xx}(\phi^{2D})$.

The relation $E_y = -d\phi^{2D}/dy$ together with eq.(6) yields:

$$-\frac{d\phi^{2D}}{dy}\rho_{xx}(\phi^{2D}) = \rho_{yx}E \quad (9)$$

Separation of the variables ϕ^{2D} and y and subsequent integration of eq.9 between two sides of the 2D conductor (y -direction) with corresponding electric potentials ϕ_1 and ϕ_2 yield the following result:

$$\rho_D(\phi_2 - \phi_1 + \frac{2A_{mis}}{\beta}[\sin[\frac{\beta}{2}(\phi_2 - \phi_1)] \times \cos[\frac{\beta}{2}(\phi_2 + \phi_1) + \theta_0]]) = \rho_{xy}EL_y \quad (10)$$

$$\beta = 4\pi\epsilon_0\epsilon\gamma/(ed_{eff}\hbar\omega_c), \\ \theta_0 = 2\pi\Delta_0/\hbar\omega_c - \beta\phi^{SL},$$

where L_y is the width of the sample. Taking into account that longitudinal voltage is $V_{xx} = EL_x$, where L_x is a distance between the potential contacts, and the Hall voltage $V_H = \phi_2 - \phi_1 = -\int E_y dy = -\rho_{yx}I$ (see eq.6), the following relation is obtained:

$$V_{xx} = R_D(I - \frac{2A_{mis}}{\beta\rho_{xy}}[\sin(\frac{\beta\rho_{xy}I}{2}) \cdot \cos[\frac{\beta}{2}(\phi_2 + \phi_1) + \theta_0]]) \quad (11)$$

, where $R_D = L_x\rho_D/L_y$ is the Drude resistance.

Eq.11 is simplified further for two cases corresponding to a minimum and a maximum of MIS-oscillations. In these cases the voltage $\phi^{2D}(\delta y) - \phi^{SL}$ is expected to be an asymmetric function of the relative position $\delta y = y - y_0$ with respect to the center of the sample y_0 (as shown in fig. 8) and, thus, $\phi_1 - \phi^{SL} = -(\phi_2 - \phi^{SL})$ and the argument of the cosine in eq.11 becomes to be independent on the electric current. In these cases the differential resistance $r_{xx} = dV_{xx}/dI$ is found to be

$$r_{xx} = R_D[1 + A_{mis} \cdot \cos(2\pi\frac{I}{I_{mis}}) \cdot \cos(\frac{2\pi\Delta_0}{\hbar\omega_c})], \quad (12)$$

where the electric current $I_{mis} = e^3\hbar d_{eff}n/\epsilon\epsilon_0 m\gamma$ determines the period of the dc bias induced oscillations. The current is proportional to the effective screening length d_{eff} and inversely proportional to the parameter γ relating variations of the sub-band energy separation Δ_{12} with variations of the electron density n in Eq.3.

Eq.12 demonstrates oscillations of the differential resistance with the electric current. The period of the oscillations I_{mis} does not depend on the magnetic field in accordance with the experiment. A similar periodicity of the resistance is found in electron systems with a single populated sub-band²¹. In this case the period of the oscillations $I_0 = (e^3 d_{eff} n)/(\pi\hbar\epsilon\epsilon_0)$ is also independent of the magnetic field and proportional to the screening length d_{eff} (see Eq.9 in Ref.²¹). In both cases the observed dependence on the screening length d_{eff} follows from the fact that an electron system with an effective screening (small d_{eff}) requires strong variations of the

electron density δn in the conducting layer to produce the same electric field (current). Thus a smaller electric current is required to depopulate a Landau level or to change the inter-band energy separation Δ_{12} in the systems with stronger screening.

The independence of the characteristic currents I_{mis} and I_0 on the magnetic field is a direct consequence of the origin of the observed phenomena. In the case of electron systems with a single band populated the resistance oscillations are induced by a variation of electron density δN_{SdH} , which is on the order of the total number of electron states in a Landau level n_0 : $\delta N_{SdH} \approx n_0 = eB/\pi\hbar \sim B$ and, thus, is proportional to the magnetic field. The variation of electron density δN_{SdH} produces Hall voltage V_H , which, due to the principle of the linear superposition of electric fields, is proportional to the density variation: $V_H = F[\delta N_{SdH}]$, where $F[x]$ is a linear functional ($A \cdot F(x) = F[Ax]$). Characteristic electric current I_0 obeys $I_0 = V_H/\rho_{xy} = (1/\rho_{xy} \cdot F[\delta N_{SdH}] = F[\delta N_{SdH}/\rho_{xy}]$. Due to the independence of the argument ($\delta N_{SdH} \sim B$)/($\rho_{xy} \sim B$) on the magnetic field B the current I_0 does not depend on the magnetic field either.

In electron systems with two populated subbands the resistance oscillations are induced by variations of the inter-subband separation Δ_{12} on the order of $\hbar\omega_c$: $\gamma\delta N_{mis} = \hbar\omega_c \sim B$. We note that in this case the characteristic scale of the electron density variations is also proportional to the magnetic field. Arguments, which are similar to one used above, yield $I_{mis} = F[\hbar\omega_c/(\gamma \cdot \rho_{xy})]$ and, as in the previous case, the characteristic electric current does not depend on the magnetic field.

The Eq.(12) indicates that the amplitude of the MIS-oscillations is strongly modulated by the dc bias. In particular at $I = I_{mis}/4$ the amplitude is zero. At this node the $1/B$ periodic oscillations change phase by π . The strong amplitude modulation with the dc bias and the π phase shift at a node agree with the experiment.

Following from Eq.(12) the positions of the nodes and anti-nodes of the oscillations with respect to the electric current I do not agree with the experiment. In accordance with Eq.(12) the nodes occurs at the averaged density of the electric current ($J = I/L_y$)

$$J_k = \frac{I_{mis}}{4L_y} \cdot k, \\ k = 2i - 1; i = 1, 2, 3, \dots, \quad (13)$$

where k is a node index. Upper panel of Fig.5 shows nodes at 0.22, 0.93, 2.41 and 3.91 A/m. Thus the relative positions of the nodes observed in the experiment do not follow the node positions (or index k) in Eq.(13). Below we show that the disagreement is reduced significantly taking into account the Joule heating.

The model discussed above does not take into account the dc heating of the 2D electrons. The Joule heating in systems with a discrete spectrum (quantal heating) has a peculiar form providing strong impact on the electron transport⁹. In electron systems with two subbands occu-

pied the quantal heating inverts the MIS-oscillations^{10,11}. A quantitative account of the heating will be done in this paper in a simplified form, taking into account an analytical approximation of the heating which is valid for two subbands with equal electron population. As shown below, the approach yields the positions of the nodes which agree with the experiment.

The expression for the resistivity of 2D electron systems with two equally populated subbands in crossed electric and quantizing magnetic field reads¹¹

$$\rho_{xx} = \rho_D [1 + \exp(-\frac{2\pi}{\omega_c \tau_q}) \frac{1-3Q}{1+Q} (1 + \cos(\frac{2\pi \Delta_{12}}{\hbar \omega_c}))] \quad (14)$$

$$Q = \frac{2\pi^3 J^2}{e^2 n \omega_c^2} \cdot \frac{\tau_{in}}{\tau_{tr}},$$

where τ_q is quantum scattering time, τ_{in} and τ_{tr} are inelastic and transport scattering times. To account for the heating we replace Eq.(7) by Eq.(14) and evaluate differential Eq.(9) numerically with fitting parameters approximating the experimental data. Due to a quite rough approximation of the heating, the fitting parameters may deviate significantly from actual physical values. To find the fitting parameter corresponding to the inelastic scattering time we use the fact that the second term of Eq.(14) is zero at $Q=1/3$ ¹¹. Assuming that at a small dc bias and low temperatures the quantal heating dominates^{9,11}, we related the first node shown in Fig.5 at $J=0.22$ A/m to the condition $Q=1/3$. This yields $\tau_{in} = 1.8$ ns at $B=0.53$ T. Using this value we solved Eq.(9) numerically. The result is shown in Fig.9 (a). At small dc bias $J \approx 0.17$ A/m the figure demonstrates the oscillation node, induced by the heating with a small contribution from the variation of the band separation Δ_{12} . Other nodes occur at considerably higher dc biases and are shifted with respect to the nodes shown in Fig.9(b)), which obtained by the numerical evaluation, ignoring the quantal heating ($Q=0$).

At $Q > 1/3$ the heating not only shift the nodes but also inverts the oscillations induced by the variation of the band separation. Namely, shown in Fig.9(a) the maximum at $J=1.75$ A/m is a result of the dc bias induced evolution of the MISO maximum at $J=0$ A/m. Without the heating the MISO maximum evolves into a minimum at $J=1.65$ A/m shown in Fig.9(b). Thus the heating inverts minimums to maximums and visa versa. The inversion is directly related to the sign change of the second term in Eq.(14) at $Q=1/3$.

The heating and the variation of the band separation affect differently the maximums and minimums of MIS-oscillations. Conversely, quantal heating decreases the resistance at any magnetic field. A variation of the resistance, induced by the change of the band separation, depends on the magnetic field. At a maximum (state P in Fig.(1)), a variation of Δ_{12} destroys the level alignment decreasing the inter-band scattering and, thus, the resistance. At a minimum (state M in Fig.(1), a variation of Δ_{12} improves the level alignment and increases the inter-band scattering and the resistance. Thus at a MISO maximum both the heating and the variations of the band

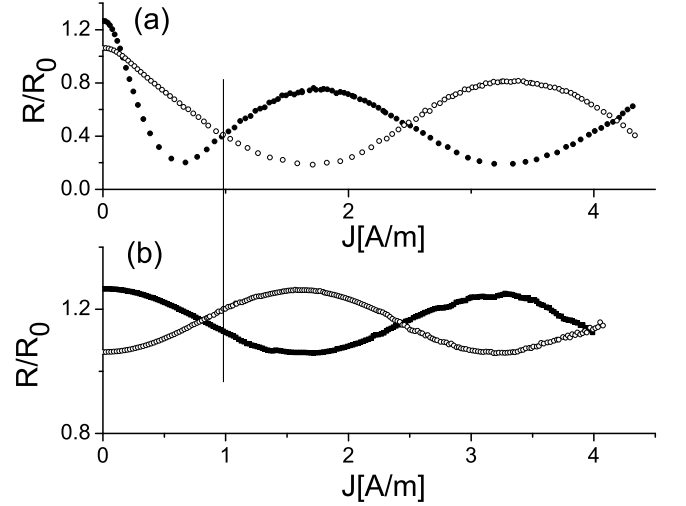


FIG. 9: (a) Numerical simulation of the dependence of differential resistance on dc bias at $B=0.53$ T. Fitting parameters used in the numerical simulation: $\tau_{in}=1.8$ ns, $\tau_q=2.5$ ps and $\tau_{tr}=45$ ps; electron density $n=8.09 \cdot 10^{15}$ 1/m²; effective screening length $d_{eff}=30$ nm; parameter $\gamma=1 \cdot 10^{-37}$ Jm² (see Eq.(3)). (b) Numerical simulation of the dependence of differential resistance on dc bias with the same fitting parameters as in (a) but without dc heating: $\tau_{in}=0$ ns ($Q=0$). Filled (open) circles present evolution of a MISO maximum (minimum) with the dc bias

separation decreases the resistance whereas at a MISO minimum two mechanisms work against each other. As a result the drop of the resistance at a MISO maximum is considerably stronger than the one at a MISO minimum. In fact, the shoulder (feature +A in Fig.3) is a result of the competition between two mechanisms at a MISO minimum whereas ZDRS states, developed from MISO maximums, is a strong indication of the joint decrease of the resistance due to both mechanisms. The behavior is reproduced in the proposed model. Indeed, Fig.9(a) shows that the initial drop of the MISO maximum is considerably stronger than the decrease of the MISO minimum with the dc bias.

Figure 10 presents a comparison of the positions of oscillation nodes, obtained in the model, with the experiment. For the purpose of a comparison, the node positions are plotted versus the index k , which is defined in Eq.(13). Without the heating, nodes of oscillations obey Eq.13. Filled triangles demonstrate this behavior. When the heating is on (filled squares), the first node ($k=1$) is due mostly to the heating. The following nodes ($k=3, 5$, and 7) are due mostly to the variation of the band separation. As shown in the figure the positions of the nodes correlate well with the experimental values (open circles) taken from the upper panel of Fig.5.

The quantal heating produces an additional node of the dc bias induced oscillations. It changes the systematic placement of the node positions described by Eq.(13). In

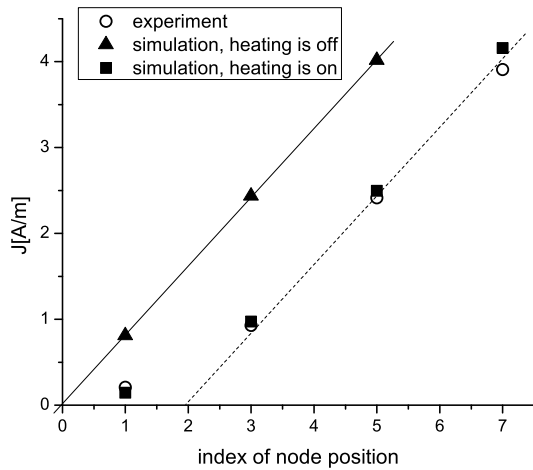


FIG. 10: Position of nodes of dc bias induced oscillations shown in Fig.9 and Fig.5 at different node index k . Filled triangles present nodes, which are obtained numerically without heating and obey Eq.(13) (solid line). Account of the heating (filled squares) improves significantly agreement with the experiment (open circles). Dashed line is a shift of the solid line to the right by two units (see text for detail).

the case of a strong quantal heating (as in Fig.9) the additional node occurs at the very beginning of the resistance evolution. Expected from Eq.(13) node counting can be largely restored by a reduction of the node index by two, which is the difference between consecutive indexes k in Eq.(13). The corresponding transformation is shown in Fig.10: the dashed line is the shift by two units to the right of the solid line representing index k in Eq.(13).

V. CONCLUSION

Quantum oscillations of nonlinear resistance, which occur in response to electric current and magnetic field applied perpendicular to GaAs quantum wells with two populated subbands, are investigated. At small magnetic fields, the current-induced oscillations are found to be related to Landau-Zener transitions between Landau levels inside the lowest subband. The period of these oscillations is proportional to the magnetic field. At high magnetic fields, a different kind of quantum oscillations are observed. With respect to the dc bias, these resistance oscillations are quasi-periodic with a period that is independent of the magnetic field. At a fixed electric current, the oscillations are periodic in inverse magnetic field. The period is independent of the *dc* bias. The proposed model considers these oscillations as a result of a joint effect between the Joule heating in the systems with discrete spectrum and the spatial variations of the energy separation between two subbands, which is induced by the electric current. The obtained results indicate the feasibility of considerable modification of the electron spectrum by applied electric current in two dimensional electron systems.

Acknowledgments

S. V. thanks I. L. Aleiner for valuable help with the theoretical model and discussion. Work was supported by National Science Foundation (DMR 1104503) and the Russian Foundation for Basic Research, project no. 11-02-00925.

* Corresponding author: vitkalov@sci.ccny.cuny.edu

† Novosibirsk State Technical University, 630092 Novosibirsk, Russia

¹ H. L. Stormer, A. C. Gossard, and W. Weigmann, Solid State Commun. **41**, 707 (1982).

² D. R. Leadley, R. Fletcher, R. J. Nicholas et al., Phys. Rev. B **46**, 12439 (1992).

³ L. I. Magarill and A. A. Romanov, Sov. Phys. Solid State **13**, 828 (1971).

⁴ V. M. Polyanovskii, Sov. Phys. Semicond. **22**, 1408 (1988).

⁵ M. E. Raikh, T. V. Shabazyan, Phys. Rev. B **49**, 5531 (1994).

⁶ A. A. Bykov, A. V. Goran, and S. A. Vitkalov, Phys. Rev. B **81**, 155322 (2010).

⁷ I. A. Dmitriev, M.G. Vavilov, I. L. Aleiner, A. D. Mirlin, and D. G. Polyakov, Phys. Rev. B **71**, 115316 (2005).

⁸ Jing-qiao Zhang, Sergey Vitkalov, A. A. Bykov, A. K. Kalagin, and A. K. Bakarov Phys. Rev. B **75**, 081305(R) (2007).

⁹ Jing Qiao Zhang, Sergey Vitkalov, and A. A. Bykov Phys. Rev. B **80**, 045310 (2009).

¹⁰ A. A. Bykov, JETP Lett. **88**, 64 (2008).

¹¹ N. C. Mamani, G. M. Gusev, O. E. Raichev, T. E. Lamas, and A. K. Bakarov, Phys. Rev. B **80**, 075308 (2009).

¹² C. L. Yang, J. Zhang, and R. R. Du, J. A. Simmons and J. L. Reno, Phys. Rev. Lett. **89**, 076801 (2002).

¹³ M.G. Vavilov, I.L. Aleiner, and L.I. Glazman, Phys. Rev. B **76**, 115331 (2007).

¹⁴ A. A. Bykov, Jing-qiao Zhang, Sergey Vitkalov, A. K. Kalagin, and A. K. Bakarov, Phys. Rev. B **72**, 245307 (2005).

¹⁵ W. Zhang, H.-S. Chiang, M. A. Zudov, L.N. Pfeiffer, and K.W. West, Phys. Rev. B **75**, 041304(R) (2007).

¹⁶ Yanhua Dai, Z. Q. Yuan, C. L. Yang, R. R. Du, M. J. Manfra, L. N. Pfeiffer, and K. W. West, Phys. Rev. B **80**, 041310 (2009).

¹⁷ A. A. Bykov, JETP Lett. **88**, 394 (2008).

¹⁸ A. A. Bykov, E. G. Mozulev, and S. A. Vitkalov, JETP Lett. **92**, 475 (2010).

¹⁹ S. Wiedmann, G. M. Gusev, O. E. Raichev, A. K. Bakarov, and J. C. Portal, Phys. Rev. B **84**, 165303 (2011).

²⁰ A. V. Goran, A. K. Kalagin, and A. A. Bykov, JETP Lett.

- 94, 535 (2011).
- ²¹ Scott Dietrich, Sean Byrnes, Sergey Vitkalov, D. V. Dmitriev and A. A. Bykov Phys. Rev. B **85**, 155307 (2012).
 - ²² K. J. Friedland, R. Hey, H. Kostial, R. Klann, and K. Ploog, Phys. Rev. Lett. **77**, 4616 (1996).
 - ²³ A. A. Bykov, J.Q. Zhang, S. Vitkalov, A. K. Kalagin, and A. K. Bakarov, Phys. Rev. Lett. **99**, 116801 (2007).
 - ²⁴ A. T. Hatke, H.-S. Chiang, M. A. Zudov, L. N. Pfeiffer, and K. W. West, Phys. Rev. B **82**, 041304(R) (2010).
 - ²⁵ G. M. Gusev, S. Wiedmann, O. E. Raichev, A. K. Bakarov, and J. C. Portal, Phys. Rev B **83**, 041306(R) (2011).
 - ²⁶ D. Shoenberg *Magnetic oscillations in metals*, (Cambridge University Press, 1984).
 - ²⁷ I. Baskin, B. M. Ashkinadze, E. Cohen, V. V. Belkov, L. N. Pfeiffer, and V. Umansky, Phys. Rev. B **84**, 245320 (2011).
 - ²⁸ A. A. Shashkin, V. T. Dolgoplov, and S. I. Dorozhkin, Sov. Phys. JETP **64**, 1124 (1986).
 - ²⁹ M. I. Dyakonov, Solid State Comm. **78**, 817 (1991).
 - ³⁰ J. M. Ziman *Principles of the theory of solids*, (Cambridge at the University Press, 1972).
 - ³¹ T. Ando, A. B. Fowler, and F. Stern, Rev. of Mod. Phys. B **54**, 437 (1982).